
ZEROS CAN BE INFORMATIVE: MASKED BINARY U-NET FOR IMAGE SEGMENTATION ON TENSOR CORES

Chunshu Wu

PNNL

Richland, WA, USA

Ruibing Song

Rice University

Houston, TX, USA

Sushant Kondguli

META

San Francisco, CA, USA

Tong Geng

Rice University

Houston, TX, USA

Ang Li

PNNL

Richland, WA, USA

ABSTRACT

Real-time image segmentation is a key enabler for AR/VR, robotics, drones, and autonomous systems, where tight accuracy, latency, and energy budgets must be met on resource-constrained edge devices. While U-Net offers a favorable balance of accuracy and efficiency compared to large transformer-based models, achieving real-time performance on high-resolution input remains challenging due to compute, memory, and power limits. Extreme quantization, particularly binary networks, is appealing for its hardware-friendly operations. However, two obstacles limit practicality: (1) severe accuracy degradation, and (2) a lack of end-to-end implementations that deliver efficiency on general-purpose GPUs.

We make two empirical observations that guide our design. (1) An explicit zero state is essential: training with zero masking to binary U-Net weights yields noticeable sparsity. (2) Quantization sensitivity is uniform across layers. Motivated by these findings, we introduce Masked Binary U-Net (MBU-Net), obtained through a cost-aware masking strategy that prioritizes masking where it yields the highest accuracy-per-cost, reconciling accuracy with near-binary efficiency.

To realize these gains in practice, we develop a GPU execution framework that maps MBU-Net to Tensor Cores via a subtractive bit-encoding scheme, efficiently implementing masked binary weights with binary activations. This design leverages native binary Tensor Core BMMA instructions, enabling high throughput and energy savings on widely available GPUs. Across 3 segmentation benchmarks, MBU-Net attains near full-precision accuracy (3% average drop) while delivering 2.04 \times speedup and 3.54 \times energy reductions over a 16-bit floating point U-Net.

1 Introduction

Image segmentation is essential for applications such as AR/VR, autonomous drones, autopilot systems, and robotics. In these domains, real-time perception and sustained operation are typically required. For instance, segmentation at roughly 60 Hz frame rate is fundamental for Meta’s AR glasses to deliver a smooth, context-aware user experience. Likewise, inspection or delivery drones often must operate continuously for 30 minutes, sometimes even hours on a single battery. Consequently, in addition to accuracy, processing speed and power efficiency are also decisive for practical deployment on edge devices. With rising demand for high-resolution data and high frame rates, these constraints have become increasingly stringent.

Compared to large, over-parameterized architectures such as Vision Transformer [1], U-Net [2] is substantially cheaper in compute, memory, and energy for dense prediction, making it a more promising choice for edge scenarios. Additionally, U-Net’s characteristic encoder-decoder structure with skip connections has demonstrated high effectiveness for pixel-level tasks [3, 4], preserving spatial details and facilitating accurate pixel-level predictions. Nevertheless, running a U-Net on high-resolution video in real time can still exceed the strict power, latency, and memory limits of many edge devices – further optimizations are necessary to reconcile accuracy with deployability.

Quantization [5, 6, 7] is a natural path to efficiency. At the extreme, binary networks [8, 9] use 1-bit weights and activations, replacing Multiply-Accumulations (MACs) with simple bitwise operations (XNOR/XOR) followed by a population count (popcount) [10]. Since most processors handle data in chunks rather than individual bits, practical implementations group many binary values together – allowing a single instruction to execute many binary operations in parallel. This approach is highly efficient on CPUs and GPU CUDA cores [11, 12], and can be further extended to exploit Tensor Cores [13]. Collectively, these techniques leverage inexpensive, hardware-friendly operations to sharply reduce compute, memory traffic, and energy, making extreme low-bit inference attractive for resource-constrained edge deployments.

However, two practical challenges hinder the effectiveness of extreme quantization. (1) **Accuracy degradation**. Binary networks usually suffer from a significant drop in accuracy due to the aggressive 1-bit quantization, and the impact on U-Net in segmentation tasks can be especially severe [14, 15]. (2) **Scarce practical solutions on general-purpose processors**. Many binary/ternary methods [16, 17, 18, 19] are algorithmic proofs-of-concept or tailored to custom FPGA [20, 21, 22] and ASIC [23] datapaths, leaving end-to-end U-Net designs and optimizations on general-purpose processors (e.g., GPUs) underexplored. To address these challenges, this paper aims to answer: (1) How to achieve near-full-precision accuracy with near-binary efficiency for U-Net on segmentation tasks? (2) How to deliver that efficiency on widely available GPUs without relying on specialized accelerators?

To address the first challenge, we design our solution based on two key observations: (1) **An explicit zero state is essential**. Pure binary representations ($\{-1, +1\}$) force every connection to contribute, offering no neutral state to suppress uncertain or noisy signals. Our experiments demonstrate that, when training with zero masking on U-Net weights, in addition to substantially enhanced accuracy, there is noticeable sparsity – over 90% zeros in many layers, some consistently exceeding 95% – far outnumbering the $+1$ and -1 states. This indicates an abundance of signals that should be suppressed by zeros. (2) **Uniform sensitivity across layers**. An exhaustive sweep over 4,000 per-layer quantization configurations shows that masking any single layer has a comparable effect on accuracy. Since masking adds overhead, and masking all layers is often unnecessary if a subset already provides sufficient suppression of information flow, low-cost layers can be prioritized for masking to balance computation and accuracy. For example, masking transposed convolution layers has a strong impact on accuracy while incurring negligible computational cost.

Since extra costs are incurred due to masking, we can strategically pick which layer to enable masking for computing and accuracy tradeoff, as it may not be necessary to apply masking for all layers, some of them can already ensure sufficient suppression for information pass. For instance, transposed convolution layers have strong impact on accuracy, despite their negligible computing cost. Guided by these findings, we propose a *cost-aware masking* strategy that identifies critical layers where masking is most beneficial, and introduce *Masked Binary U-Net* (MBU-Net), which achieves **near full-precision accuracy with near-binary efficiency** as highlighted in Figure 1.

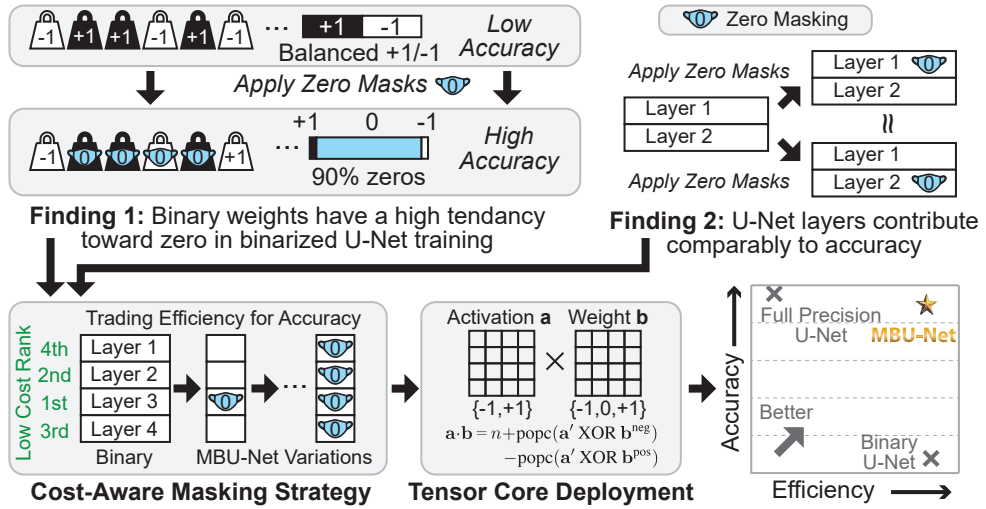


Figure 1: Overview. Obtained through a cost-aware masking strategy and optimized for Tensor Core on GPUs, MBU-Net achieves full-precision level accuracy and binary-level efficiency.

To address the second challenge, we target Tensor Cores, mapping MBU-Net via bit-packing and dedicated APIs. On GPUs with Tensor Cores, performance is typically memory-bound rather than compute-bound, thus we retain binary activations to reduce data movement and power. This approach is timely: Tensor Cores are now common even on edge GPUs (e.g., NVIDIA Jetson Xavier with Volta Tensor Cores, Jetson Orin with Ampere Tensor Cores), positioning them as practical platforms for efficient edge application deployment. Although prior frameworks have accelerated pure

Binary Neural Networks (BNNs) on GPUs [11, 13], to the best of our knowledge, no high-performance framework exists for selectively masked binary models on Tensor Cores, especially for U-Net. To bridge this gap, we introduce a *subtractive bit-encoding* method that naturally realizes masked binary weights with binary activations within the Tensor Core paradigm, thereby unlocking **substantial efficiency gains on modern commodity GPUs**. Our major contributions are listed below.

1. We discover that: (1) An explicit zero masking state in the weights of a binary U-Net can significantly improve the segmentation quality, closely approaching full-precision results. (2) Despite being cheap, transposed convolution layers are accuracy-critical.
2. We employ a cost-aware masking strategy based on above discoveries, systematically identifying the most critical layers in a U-Net, leading to MBU-Net models that regain near full-precision segmentation accuracy at minor masking cost over a pure BNN.
3. We design and implement an end-to-end acceleration framework with native BMMA binary Tensor Core instructions through subtractive bit-encoding method, enabling unified and high-throughput inference for MBU-Net models on GPU Tensor Cores.
4. Our approach delivers an average $2.04\times$ speedup and $3.54\times$ power efficiency improvement over a 16-bit floating point U-Net on A100, H100, Jetson Orin Nano, and RTX 2080 Ti GPUs, while incurring only 3% average accuracy loss on 3 segmentation datasets. The U-Net contains 16M parameters, and the input images range from 0.25M to 0.6M pixels.

2 Backgrounds

2.1 U-Net

Since its introduction in 2015 [2], the U-Net architecture has proven to be far more than just a successful model for biomedical image segmentation [24, 25]. It has been extended to other domains including image enhancement [26], generative AI [27, 28, 29], scientific modeling [30, 31], etc.

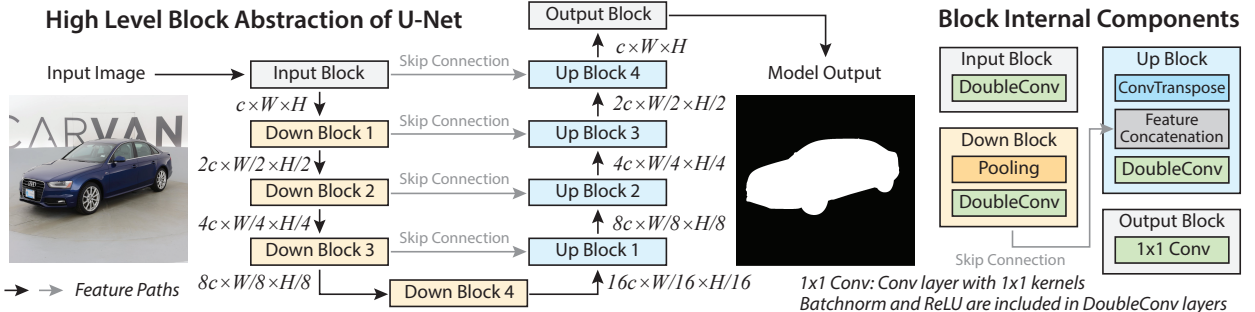


Figure 2: Left: Conventional U-Net architecture exemplified with segmentation task. c : number of channels, W/H : feature width / height. Right: internal components of each abstracted block.

At its core, as Figure 2 illustrates, U-Net is a symmetric encoder-decoder architecture linked by skip connections. The encoder (contracting path with orange down blocks) follows the typical structure of a convolutional network, downsampling the input to capture semantic context. The decoder (expanding path with blue up blocks), in return, progressively upsamples and refines the feature representations to construct a full-resolution image. To avoid forcing all information through a narrow bottleneck, skip connections concatenate encoder features with the corresponding decoder features after transposed convolution layers, passing information along multiple paths and elegantly preserving information at different semantic hierarchies.

Despite its widespread use, U-Net’s computational footprint at real-time, high-resolution settings is substantial. A configuration at 720p can require on the order of hundreds of GFLOPs per frame, and sustaining 60 fps implies tens of TFLOPs per second plus heavy memory bandwidth from skip connections. On edge platforms such as AR glasses and drones, on-device inference is often necessary for latency, privacy, and reliability, yet power budgets are only a few watts. These constraints motivate aggressive quantization and sparsity to reduce arithmetic and bandwidth while preserving accuracy. We therefore investigate U-Net in the binarized regime, aiming to characterize its behavior under extreme precision reduction and masking, and to provide guidance for edge-oriented designs that balance accuracy, compute, and energy.

2.2 Binary Neural Networks

The success of Deep Neural Networks (DNNs) has been largely predicated on a trend of escalating model complexity. In contrast, BNNs [8] shrinks the complexity to an extreme extent, with both activations and weights constrained to binary values, typically represented as $\{-1, +1\}$. For activations, this constraint is commonly enforced through a binarization function $x_b = \text{sign}(x)$ during forward pass, whereas the weights are trained under binary representation, typically using Straight-Through Estimators (STE) [32, 33, 34] to approximate the gradient in such non-differentiable architecture. Despite the low resolution, theoretical analysis [35] has confirmed BNN’s capability of capturing features.

For efficient practical deployment, XNOR-Net [10] was introduced. Specifically, for binary vectors $\mathbf{a}|a_i \in \{-1, +1\}$ and $\mathbf{b}|b_i \in \{-1, +1\}$, their MAC operation can be translated into bit-wise operations and population count on bit vectors $\mathbf{a}'|a'_i \in \{0, 1\}$ and $\mathbf{b}'|b'_i \in \{0, 1\}$:

$$\mathbf{a} \cdot \mathbf{b} = \sum_i^n (2a'_i - 1)(2b'_i - 1) = 2 \cdot \text{popc}(\mathbf{a}' \text{ XNOR } \mathbf{b}') - n \quad (1)$$

using the equality $a'_i \text{ XNOR } b'_i = 2a'_i b'_i - a'_i - b'_i$. Here, “popc” refers to population count operation that counts the number of 1’s in an n -bit vector, e.g., a 32-bit vector as an unsigned integer.

In the past decade, BNN researches follow two main threads. On the algorithmic level, researchers strive to improve BNN training accuracy, while on the implementation level, the main target is to minimize power and latency, especially on FPGA and ASIC. In this work, our goal is to push the boundaries on both directions for U-Net, achieving near full-precision accuracy with near-binary efficiency.

2.3 Tensor Core APIs

Tensor Cores are specialized units that accelerate Matrix Multiply-Accumulate (MMA), computing $D = A \times B + C$ per instruction, where A, B, C , and D are matrices of compatible dimensions. Compared with issuing many MACs on CUDA cores, a single MMA instruction performs a large number of fused operations on a small matrix tile. Impressively, for example, the throughput of Tensor Cores on A100 is almost an order of magnitude higher than CUDA cores, emphasizing the trend of shifting AI workloads to such dedicated matrix engines for higher throughput and efficiency.

In GPUs, processing units are grouped into warps, and the above MMA is executed using the WMMA API with the following three key functions: (1) Load data from memory to registers. (2) Perform the above MMA operation. (3) Write the data back to memory. Less widely known, some NVIDIA GPUs also expose bit MMA (namely, BMMA): Tensor Core instructions that compute binary matrix products using bitwise logic (e.g., XOR/AND) with popcount accumulation. These binary Tensor Core features remain low-level and experimental, as they are not exposed by mainstream libraries (e.g., cuBLAS, cuDNN) and typically require custom kernels. Consequently, despite their potential, binary Tensor Core capabilities remain underused and underexplored in practice.

In this work, we extend the scope of an existing BNN acceleration framework [36, 13] on Tensor Core, bringing the unique BMMA capability under the spotlight.

3 Methods

In this section, we present MBU-Net, a class of masked binary U-Nets inspired from empirical observations (§3.1.1) and constructed using a cost-aware masking strategy §3.1.2, achieving balanced tradeoff between accuracy and computational cost. Next, we demonstrate that with subtractive bit encoding §3.2.1, masked layers can be naturally mapped to Tensor Cores by reusing the BNN mapping §3.2.2, enabling an end-to-end implementation that runs efficiently on modern edge GPUs.

3.1 Masked Binary U-Net

3.1.1 Empirical Observations and Analysis

We begin by defining a U-Net backbone with 12 abstracted configurable layers: $4 \times$ double convolution layers in the encoder, labeled as down-C1~4; $4 \times$ transposed convolution layers in the decoder, as up-CT1~4; $4 \times$ double convolution layers in the decoder, as up-T1~4. The indexing is consistent with the block indices in Figure 2. Each layer can be instantiated in one of two states: binary or masked (i.e., with an explicit zero state in the weights), resulting in a 2^{12} design space. In the exhaustive sweeping, Carvana dataset [37] is used as a representative example.

In binary layers, input features, output features, and weights are all binary values within $\{-1, +1\}$, following the convention of BNNs. In masked layers, an masking state '0' is included in weights, effectively making the weights ternary $\{-1, 0, +1\}$, while keeping input and output features binary. Detailed network architecture is in Appendix A.1. Extensive investigations (Appendix A.2) demonstrate that higher-bit weight quantizations only result in marginal improvement compared to binary weights with masks. Through STE training approach, the zero masking is automatically applied. The training configuration is in Appendix A.3.

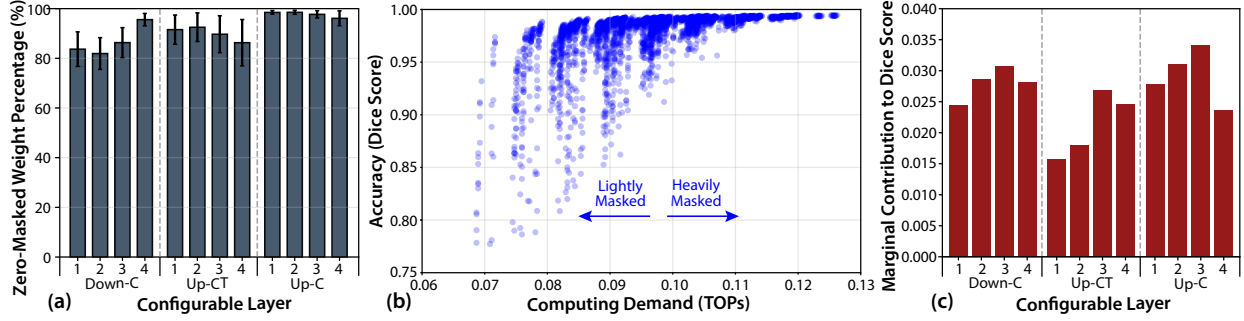


Figure 3: (a) Statistics of the weights masked to zero. (b) Accuracy and computing demand distribution for all layer configurations. (c) Shapley analysis: marginal improvement in Dice score from masking each binary layer. Only cases with fewer than five masked layers are included for clarity.

Figure 3(a) demonstrates that zero weights are notably prevalent across all masked layers and configurations. On average, each layer exhibits more than 80% sparsity, with many layers exceeding 90% and some consistently surpassing 95%. This finding indicates that it is preferable to mask out the majority of weights while retaining only a small essential subset. Figure 3(b) supports this observation: layer configurations with heavier masking generally achieve higher Dice scores (from 0 to 1, higher is better), confirming the value of masked binary weights.

However, masking inevitably introduces additional costs, which can sometimes be heavy in computation. Figure 3(b) further shows that fully masking all layers can require about twice as many operations as lightly masked configurations. Meanwhile, a configuration requiring 0.08 TOPs can achieve accuracy comparable with the fully masked configuration exceeding 0.12 TOPs. This indicates that masking every layer is unnecessary when a small set of critical layers suffices, motivating us to identify those layers to achieve high accuracy at low cost.

Figure 3(c) shows the marginal gain in Dice score for each layer under zero masking. For clarity, we restrict the analysis to cases with fewer than 5 masked layers, since including more layers dilutes the per-layer contribution due to the limited improvement in Dice score. Interestingly, the contributions are broadly comparable across layers. This observation brings a straightforward yet practical strategy: prioritize masking low-cost layers.

3.1.2 Cost-Aware Masking Strategy

The above empirical findings indicate that if some layers are significantly cheaper than others, masking the cheap layers can achieve substantial improvement in accuracy at minimal cost. We thus further profile the per-layer computing and memory in Figure 4, where the operations account for both multiplications and additions.

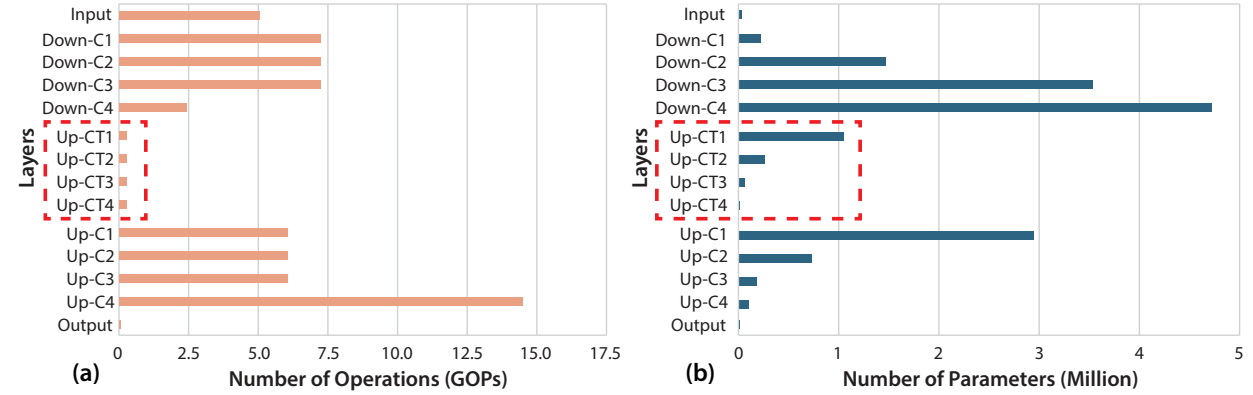


Figure 4: Per-layer cost profiling. (a) Number of addition and multiplication operations in each layer with a 512×512 image as a representative example. (b) Number of parameters in each layer.

We observe that, the numbers of operations of transposed convolution layers (highlighted with red dashed frame) in the upsampling path are 1~2 orders of magnitude fewer compared to other layers, and the operation count and parameter count are relatively imbalanced across layers. As it is usually infeasible to perform analysis like Figure 3 across the entire design space, it is preferable to set up the strategy based on the model characteristics in Figure 4. Particularly, we define the cost-aware strategy using the weighted cost score for layer l :

$$s_{\text{cost}}^l = w_{\text{op}} \hat{n}_{\text{op}}^l + w_{\text{param}} \hat{n}_{\text{param}}^l \quad (2)$$

where \hat{n}_{op}^l and \hat{n}_{param}^l are the number of operations and the number of parameters of layer l normalized to $[0, 1]$, and the weights w_{op} and w_{param} satisfy $w_{\text{op}} + w_{\text{param}} = 1$, as hyperparameters. The weighted cost scores are then ranked from low to high as the priority list for masking. Following the strategy, MBU-Net can be populated based on the priority list based on demand, narrowing down the design space significantly.

3.2 Tensor Core Deployment

3.2.1 Subtractive Bit-Encoding

MBU-Net maintains binary activations and assigns each layer to either binary or masked weights according to the cost-aware strategy described above. To ensure that the MAC between binary activation and masked weight can be naturally supported by native operations on Tensor Cores – XOR and popcount, we encode masked weights with two subtracting bit-planes. In particular, let $\mathbf{a}|a_i \in \{-1, +1\}$ denote a binary activation vector, and $\mathbf{b}|b_i \in \{-1, 0, +1\}$ as a masked weight vector, we encode a weight value as $b_i = b_i^{\text{pos}} - b_i^{\text{neg}}$, with $b_i^{\text{pos}}, b_i^{\text{neg}} \in \{0, 1\}$. The MAC operation is thus translated using $a'_i \in \{0, 1\}$:

$$\mathbf{a} \cdot \mathbf{b} = \sum_i^n \underbrace{2a'_i b_i^{\text{pos}} - b_i^{\text{pos}} - a'_i + a'_i + b_i^{\text{neg}} - 2a'_i b_i^{\text{neg}}}_{1 - (a'_i \text{ XOR } b_i^{\text{pos}})} = n + \text{popc}(\mathbf{a}' \text{ XOR } \mathbf{b}^{\text{neg}}) - \text{popc}(\mathbf{a}' \text{ XOR } \mathbf{b}^{\text{pos}}) \quad (3)$$

Compared to Equation 1, the binary-ternary MAC operation is fully represented by bit-friendly operations, only to use XOR instead of XNOR to be compatible with Tensor Core intrinsics.

3.2.2 Mapping Layers to Tensor Core

We map these computations to GPU Tensor Cores using binary WMMA, or the experimental BMMA API. Each kernel of a masked layer stores the two bit planes as bit-packed matrices. At warp level, we operate on $8 \times 8 \times 128$ bit tiles, where the three dimensions are mapped to batch size, output layer number, and input layer number. For clarity, we show the high-level procedure for convolution on Tensor Core in Algorithm 3.2.2.

Algorithm 1 Bit Convolution with Subtractive Bit-Encoding on Tensor Core

```

1: for all  $H, W, C_{\text{out}}, B$  do ▷ feature height, width, output channel, batch size
2:   Initialize accumulators  $C^{\text{pos}}, C^{\text{neg}} \leftarrow 0$ 
3:   for all  $F_H, F_W$ , and  $C_{\text{in}}$  of 128-bit blocks do ▷ filter height, width, input channel
4:     Load binary activation fragment  $A$  ▷ row-major
5:     Load binary weight fragments  $B_{\text{pos}}, B_{\text{neg}}$  ▷ column-major
6:      $\text{bmma\_sync}(C^{\text{pos}}, A, B^{\text{pos}}, C^{\text{pos}})$  ▷ binary WMMA API
7:      $\text{bmma\_sync}(C^{\text{neg}}, A, B^{\text{neg}}, C^{\text{neg}})$ 
8:   end for
9:    $R \leftarrow C^{\text{neg}} - C^{\text{pos}}$  ▷ temporary result  $R$ 
10:  Threshold comparison:  $A_{\text{out}} \leftarrow (R \geq \theta)$  ▷ covering batchnorm, bias, and binary activation
11:  Pack bits via intrinsics (ballot, brev) and store to memory
12: end for

```

In the algorithm, the matrices A , B , and C follow the update rule $C \leftarrow A \cdot B + C$, implemented using the Tensor Core API function “bmma_sync”. The function is further compiled to a Parallel Thread Execution (PTX) Tensor Core opcode that includes XOR and popcount. θ denotes the pre-computed threshold. The threshold comparison jointly incorporates batch normalization [38], bias, and binary activation, which is a standard practice in BNNs. In terms of other layers (detailed in Figure 2), transposed convolution is performed similarly, while pooling and 1×1 convolutions are trivial, hence not discussed in further details.

4 Experimental Results

4.1 Experimental Setup

Our experiments are conducted on 4 Nvidia GPU platforms: *A100* (Ampere architecture), *H100* (Hopper), *Jetson* Orin Nano (Ampere), and *RTX 2080 Ti* (Turing), all equipped with Tensor Cores. We evaluate models under the following execution settings: *PyTorch-FP32/FP16* – baseline implementations in PyTorch [39] using 32-bit floating point and 16-bit floating point for both weights and activations, where the FP16 variant employs tensor cores; *MBU-Net* adopts binary activation and mixed binary/masked weights; The *Binary* model uses both binary activations and weights. The first and the last convolution layers in the quantized experiments are full-precision. For benchmarks, we use 3 representative datasets: *Carvana* [37] – car image segmentation, *ISIC* [40] – skin lesion image segmentation, and *Nuclei* – nuclei segmentation in divergent images [41]. Dataset details are in Appendix A.3.

4.2 Efficiency Comparison

We compare separate GPU and execution settings over the selected datasets. Efficiency is evaluated and discussed in terms of latency and energy in the following sections.

4.2.1 Latency Comparison

Figure 5 shows the latency comparison. *MBU-Net* consistently outperforms FP32, with an average speedup of $4.83 \times$ over all platforms and datasets. On average, *MBU-Net* also outperforms FP16 with a $2.04 \times$ speedup. Noticeably, FP16 achieves better latency results, even compared to *Binary*. This is likely due to the removal of native BMMA support on Nvidia Hopper Tensor Core architecture [42] – performance is lost, despite *MBU-Net* and *Binary* models are still runnable.

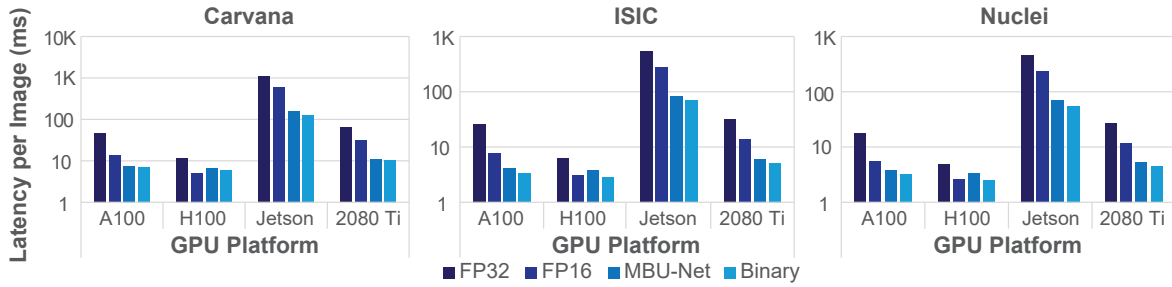


Figure 5: Latency per image inference (milliseconds). Lower is better.

4.2.2 Energy Comparison

Figure 6 presents the energy comparison. Consistently, *MBU-Net*’s energy cost is comparable to the *Binary* model, while achieving average energy reduction of $8.53 \times$ over FP32 and $3.54 \times$ over FP16.

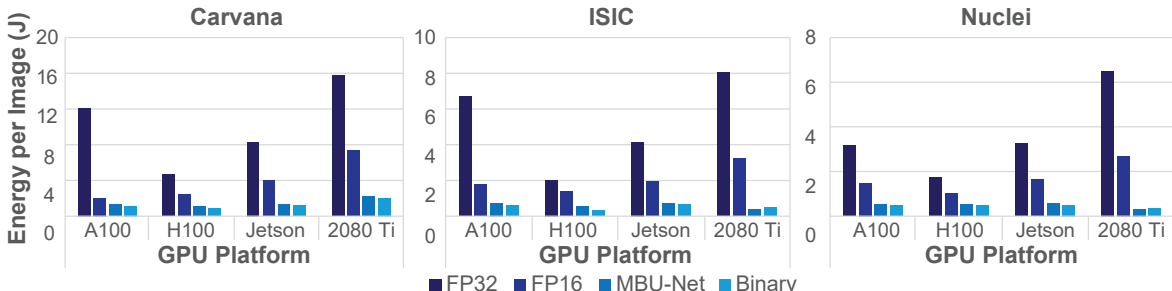


Figure 6: Energy per image inference (Joule). Lower is better.

4.3 Accuracy Comparison

Table 1 compares the U-Net model across different precision configurations. “Full Precision” refers to both full-precision weights and activations (FP32 and FP16 show negligible accuracy differences), while other configurations employ binary activations. Accuracy is evaluated with three metrics: Dice Score, IoU, and F1 score, with our results highlighted in the shaded row. On average, aggressive quantization in *MBU-Net* only leads to drops of 0.029, 0.037, and 0.024 in Dice, IoU, and F1 scores.

Table 1: Accuracy comparison using Dice score, IoU, and F1 score across three datasets. All metrics range from 0 to 1, higher is better. All configurations other than Full Precision use binary activations.

Dataset	Carvana			ISIC			Nuclei		
Metric (Weight-Activation)	Dice	IoU	F1	Dice	IoU	F1	Dice	IoU	F1
Full Precision*	0.997	0.994	0.997	0.771	0.644	0.783	0.867	0.776	0.874
INT8	0.994	0.987	0.994	0.763	0.633	0.776	0.823	0.741	0.851
INT4	0.989	0.979	0.989	0.753	0.619	0.765	0.819	0.739	0.850
MBU-Net	0.981	0.963	0.981	0.750	0.617	0.763	0.817	0.722	0.839
Binary	0.662	0.530	0.693	0.560	0.399	0.570	0.434	0.302	0.464

* Both weights and activations are in full precision; negligible difference between FP32 and FP16 accuracy.

4.4 Ablation Study

Figure 7 presents the Pareto frontier illustrating the tradeoff between accuracy (Dice score) and speed (FPS) across different MBU-Net configurations on A100 GPU, where masked layers are chosen using the cost-aware masking strategy with $w_{\text{op}} = w_{\text{param}} = 0.5$. The corresponding cost score ranking and additional results with other metrics are in Appendix A.4

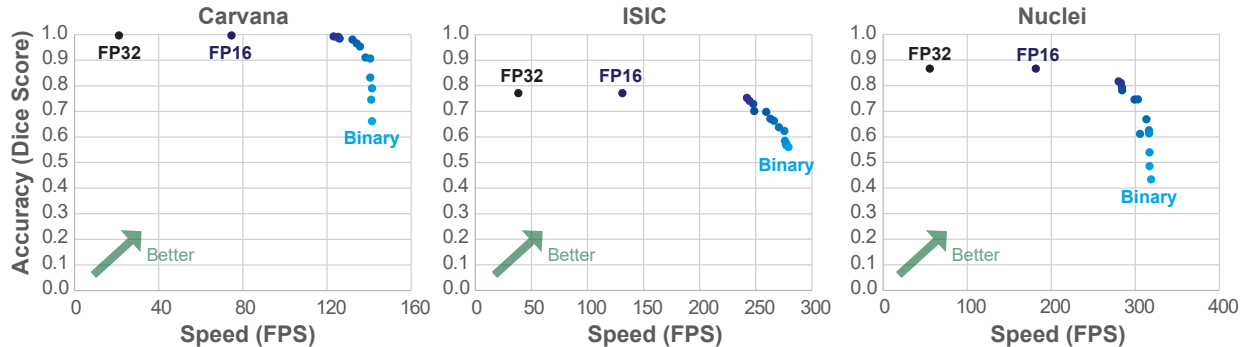


Figure 7: Pareto frontier of accuracy (dice score) and speed (FPS) on A100 for 3 datasets. Colors (bright \rightarrow dark) indicate more layers get masked, based on the cost-aware masking strategy in §3.1.2.

5 Related Work

Ternary Networks. Table 5 summarizes a few notable studies related to neural networks with ternary activations or weights. TWN [43] and TTQ [44] focus on full precision activation and ternary weights on the algorithmic level, reporting results primarily on image classification tasks. TBN [16] adopts ternary activations and binary weights, also at the algorithmic level. TernaryNet [17] is also an algorithmic endeavor, focusing on achieving faster inference without GPUs. FATNN [45] introduces a 2-bit encoding method: $-1 \rightarrow 00; 0 \rightarrow 01/10, +1 \rightarrow 11$ and uses a series of bit operations to reduce ternary-ternary operation complexity from $O(4N)$ to $O(2N)$. TAB [18] proposes a flexible framework accommodating various activation/weight quantization schemes. To our knowledge, none of these works analyze per-layer contributions to accuracy, assess compatibility with U-Net, or deliver end-to-end implementations targeting Tensor Cores on commodity GPUs.

Table 2: Summary of ternary activation/weight network studies.

Related Work	TWN	TTQ	TBN	TernaryNet	FATNN
Platform	Unspecified	Unspecified	Unspecified	CPU	GPU
Focus	Acc*	Acc	Acc & Theoretical Speed	Acc	Acc & Speed
Activation	Full Precision	Full Precision	Ternary	Ternary	Ternary
Weights	Ternary	Ternary	Binary	Ternary	Ternary
Task	IC*	IC	IC	Segmentation	IC

* IC: Image Classification; Acc: Accuracy

Image Segmentation. U-Net [2] stands as one of the most influential architectures in image segmentation, inspiring a wide range of successors that refine different aspects of its design. U-Net++ [4] introduces nested and dense skip connections. UNet3+ [46] extends this idea with full-scale skip connections. Beyond architectural refinements, U-Net is often combined with other mechanisms. Attention U-Net [47] integrates attention gates into skip connections, while ResUNet [48] and Recurrent Residual U-Net [49] incorporate residual connections to enhance the capacity of deeper networks. In the era of large models, Transformer-based approaches, notably ViTs [1], have proven effective for

segmentation tasks [50]. Segment Anything Models [51, 52], based on ViT, achieve exceptional segmentation quality. However, their parameter counts and computational demands pose significant challenges for edge deployment.

Additional Applications of U-Net. In addition to segmentation, U-Net has been widely explored for image enhancement tasks, including denoising [53, 54] and super-resolution [55]. With the rapid growth of AR/VR, U-Net has emerged as a promising candidate for waveguide correction [56] to enable lower power consumption and reduced distortions in AR systems. Moreover, U-Net plays a pivotal role in generative AI, serving as the backbone for models such as DDPM [27] and high-resolution image synthesis [57].

6 Conclusion

In this work, we address the challenges of bringing binary quantization to U-Net for real-time image segmentation on edge devices. Two critical observations are identified: (1) The necessity of an explicit zero state to suppress noisy signals and promote sparsity, and (2) the uniform sensitivity of U-Net layers to quantization. Building on these insights, we propose a cost-aware masking strategy that balances accuracy and efficiency, resulting in Masked Binary U-Net (MBU-Net). To realize its benefits on commodity hardware, we develop a GPU execution framework that leverages Tensor Cores through a subtractive bit-encoding scheme, efficiently supporting masked binary weights with binary activations. This framework ensures high throughput and power efficiency, while remaining deployable on widely available edge GPUs.

Experiments across multiple segmentation datasets demonstrate that MBU-Net achieves near full-precision accuracy (3% drop on average), while attaining $2.04\times$ speedup and $3.54\times$ energy consumption compared to a 16-bit floating point U-Net. These results establish MBU-Net as a practical and scalable solution for real-time, high-resolution image segmentation on Tensor Cores. If deployed on AR/VR, autonomous drones or related domains, this can raise a 30 FPS pipeline to 60 FPS, and cut segmentation power by 70%, extending battery life. While measured on GPU Tensor Cores, MBU-Net is well suited for ASICs: its low-bit width arithmetic and masking enable narrow data paths and reduced SRAM bandwidth, yielding higher performance per watt and deterministic latency in a dedicated accelerator.

References

- [1] Alexey Dosovitskiy, Lucas Beyer, Alexander Kolesnikov, Dirk Weissenborn, Xiaohua Zhai, Thomas Unterthiner, Mostafa Dehghani, Matthias Minderer, Georg Heigold, Sylvain Gelly, et al. An image is worth 16x16 words: Transformers for image recognition at scale. *arXiv preprint arXiv:2010.11929*, 2020.
- [2] Olaf Ronneberger, Philipp Fischer, and Thomas Brox. U-net: Convolutional networks for biomedical image segmentation. In *International Conference on Medical image computing and computer-assisted intervention*, pages 234–241. Springer, 2015.
- [3] Liang-Chieh Chen, Yukun Zhu, George Papandreou, Florian Schroff, and Hartwig Adam. Encoder-decoder with atrous separable convolution for semantic image segmentation. In *Proceedings of the European conference on computer vision (ECCV)*, pages 801–818, 2018.
- [4] Zongwei Zhou, Md Mahfuzur Rahman Siddiquee, Nima Tajbakhsh, and Jianming Liang. Unet++: Redesigning skip connections to exploit multiscale features in image segmentation. *IEEE transactions on medical imaging*, 39(6):1856–1867, 2019.
- [5] Amir Gholami, Sehoon Kim, Zhen Dong, Zhewei Yao, Michael W Mahoney, and Kurt Keutzer. A survey of quantization methods for efficient neural network inference. In *Low-power computer vision*, pages 291–326. Chapman and Hall/CRC, 2022.
- [6] Lu Wei, Zhong Ma, Chaojie Yang, and Qin Yao. Advances in the neural network quantization: A comprehensive review. *Applied Sciences*, 14(17):7445, 2024.
- [7] Pouya Haghi, Chunshu Wu, Zahra Azad, Yanfei Li, Andrew Gui, Yuchen Hao, Ang Li, and Tony Tong Geng. Bridging the gap between ILMs and LNs with dynamic data format and architecture codesign. In *2024 57th IEEE/ACM International Symposium on Microarchitecture (MICRO)*, pages 1617–1631. IEEE, 2024.
- [8] Itay Hubara, Matthieu Courbariaux, Daniel Soudry, Ran El-Yaniv, and Yoshua Bengio. Binarized neural networks. *Advances in neural information processing systems*, 29, 2016.
- [9] Zechun Liu, Zhiqiang Shen, Marios Savvides, and Kwang-Ting Cheng. Reactnet: Towards precise binary neural network with generalized activation functions. In *European conference on computer vision*, pages 143–159. Springer, 2020.

[10] Mohammad Rastegari, Vicente Ordonez, Joseph Redmon, and Ali Farhadi. Xnor-net: Imagenet classification using binary convolutional neural networks. In *European conference on computer vision*, pages 525–542. Springer, 2016.

[11] Ang Li, Tong Geng, Tianqi Wang, Martin Herbordt, Shuaiwen Leon Song, and Kevin Barker. Bstc: A novel binarized-soft-tensor-core design for accelerating bit-based approximated neural nets. In *Proceedings of the international conference for high performance computing, networking, storage and analysis*, pages 1–30, 2019.

[12] Jou-An Chen, Hsin-Hsuan Sung, Xipeng Shen, Sutanay Choudhury, and Ang Li. Bitgnn: Unleashing the performance potential of binary graph neural networks on gpus. In *Proceedings of the 37th International Conference on Supercomputing*, pages 264–276, 2023.

[13] Ang Li and Simon Su. Accelerating binarized neural networks via bit-tensor-cores in turing gpus. *IEEE Transactions on Parallel and Distributed Systems*, 32(7):1878–1891, 2020.

[14] MohammadHossein AskariHemmat, Sina Honari, Lucas Rouhier, Christian S Perone, Julien Cohen-Adad, Yvon Savaria, and Jean-Pierre David. U-net fixed-point quantization for medical image segmentation. In *International Workshop on Large-scale Annotation of Biomedical data and Expert Label Synthesis*, pages 115–124. Springer, 2019.

[15] Liming Guo, Wen Fei, Wenrui Dai, Chenglin Li, Junni Zou, and Hongkai Xiong. Mixed-precision quantization of u-net for medical image segmentation. In *2022 IEEE International Symposium on Circuits and Systems (ISCAS)*, pages 2871–2875. IEEE, 2022.

[16] Diwen Wan, Fumin Shen, Li Liu, Fan Zhu, Jie Qin, Ling Shao, and Heng Tao Shen. Tbn: Convolutional neural network with ternary inputs and binary weights. In *Proceedings of the European Conference on Computer Vision (ECCV)*, pages 315–332, 2018.

[17] Mattias P Heinrich, Max Blendowski, and Ozan Oktay. Ternarynet: faster deep model inference without gpus for medical 3d segmentation using sparse and binary convolutions. *International journal of computer assisted radiology and surgery*, 13(9):1311–1320, 2018.

[18] Shien Zhu, Luan HK Duong, and Weichen Liu. Tab: Unified and optimized ternary, binary, and mixed-precision neural network inference on the edge. *ACM Transactions on Embedded Computing Systems (TECS)*, 21(5):1–26, 2022.

[19] Rui Yin, Haotong Qin, Yulun Zhang, Wenbo Li, Yong Guo, Jianjun Zhu, Cheng Wang, and Biao Jia. Bidense: Binarization for dense prediction. *arXiv preprint arXiv:2411.10346*, 2024.

[20] Shuang Liang, Shouyi Yin, Leibo Liu, Wayne Luk, and Shaojun Wei. Fp-bnn: Binarized neural network on fpga. *Neurocomputing*, 275:1072–1086, 2018.

[21] Tong Geng, Tianqi Wang, Chunshu Wu, Chen Yang, Shuaiwen Leon Song, Ang Li, and Martin Herbordt. Lp-bnn: Ultra-low-latency bnn inference with layer parallelism. In *2019 IEEE 30th International Conference on Application-specific Systems, Architectures and Processors (ASAP)*, volume 2160, pages 9–16. IEEE, 2019.

[22] VRS Mani, A Saravanaselvan, and NJMJ Arumugam. Performance comparison of cnn, qnn and bnn deep neural networks for real-time object detection using zynq fpga node. *Microelectronics Journal*, 119:105319, 2022.

[23] Ankit Wagle, Sunil Khatri, and Sarma Vrudhula. A configurable bnn asic using a network of programmable threshold logic standard cells. In *2020 IEEE 38th International Conference on Computer Design (ICCD)*, pages 433–440. IEEE, 2020.

[24] Nabil Ibtehaz and M Sohel Rahman. Multiresunet: Rethinking the u-net architecture for multimodal biomedical image segmentation. *Neural networks*, 121:74–87, 2020.

[25] Junlong Cheng, Shengwei Tian, Long Yu, Shijia Liu, Chaoqing Wang, Yuan Ren, Hongchun Lu, and Min Zhu. Ddu-net: A dual dense u-structure network for medical image segmentation. *Applied Soft Computing*, 126:109297, 2022.

[26] Rina Komatsu and Tad Gonsalves. Comparing u-net based models for denoising color images. *AI*, 1(4):465–486, 2020.

[27] Jonathan Ho, Ajay Jain, and Pieter Abbeel. Denoising diffusion probabilistic models. *Advances in neural information processing systems*, 33:6840–6851, 2020.

[28] Edgar Schonfeld, Bernt Schiele, and Anna Khoreva. A u-net based discriminator for generative adversarial networks. In *Proceedings of the IEEE/CVF conference on computer vision and pattern recognition*, pages 8207–8216, 2020.

[29] Chenyang Si, Ziqi Huang, Yuming Jiang, and Ziwei Liu. Freeu: Free lunch in diffusion u-net. In *Proceedings of the IEEE/CVF Conference on Computer Vision and Pattern Recognition*, pages 4733–4743, 2024.

[30] Ali Kamali and Kaveh Laksari. Physics-informed unets for discovering hidden elasticity in heterogeneous materials. *Journal of the mechanical behavior of biomedical materials*, 150:106228, 2024.

[31] Tong Zhu, Dehao Liu, and Yanglong Lu. Finite-volume physics-informed u-net for flow field reconstruction with sparse data. *Journal of Computing and Information Science in Engineering*, 25(7):071004, 2025.

[32] Yoshua Bengio, Nicholas Léonard, and Aaron Courville. Estimating or propagating gradients through stochastic neurons for conditional computation. *arXiv preprint arXiv:1308.3432*, 2013.

[33] Matthieu Courbariaux, Yoshua Bengio, and Jean-Pierre David. Binaryconnect: Training deep neural networks with binary weights during propagations. *Advances in neural information processing systems*, 28, 2015.

[34] Penghang Yin, Jiancheng Lyu, Shuai Zhang, Stanley Osher, Yingyong Qi, and Jack Xin. Understanding straight-through estimator in training activation quantized neural nets. *arXiv preprint arXiv:1903.05662*, 2019.

[35] Alexander G Anderson and Cory P Berg. The high-dimensional geometry of binary neural networks. *arXiv preprint arXiv:1705.07199*, 2017.

[36] Morteza Hosseini, Hirenkumar Paneliya, Utteja Kallakuri, Mohit Khatwani, and Tinoosh Mohsenin. Minimizing classification energy of binarized neural network inference for wearable devices. In *20th International Symposium on Quality Electronic Design (ISQED)*, pages 259–264. IEEE, 2019.

[37] Brian Shaler, Dan Gill, Maggie McDonald, Patricia, and Will Cukierski. Carvana image masking challenge. <https://kaggle.com/competitions/carvana-image-masking-challenge>, 2017. Kaggle.

[38] Sergey Ioffe and Christian Szegedy. Batch normalization: Accelerating deep network training by reducing internal covariate shift. In *International conference on machine learning*, pages 448–456. pmlr, 2015.

[39] Adam Paszke, Sam Gross, Francisco Massa, Adam Lerer, James Bradbury, Gregory Chanan, Trevor Killeen, Zeming Lin, Natalia Gimelshein, Luca Antiga, et al. Pytorch: An imperative style, high-performance deep learning library. *Advances in neural information processing systems*, 32, 2019.

[40] Noel Codella, Veronica Rotemberg, Philipp Tschandl, M Emre Celebi, Stephen Dusza, David Gutman, Brian Helba, Aadi Kalloo, Konstantinos Liopyris, Michael Marchetti, et al. Skin lesion analysis toward melanoma detection 2018: A challenge hosted by the international skin imaging collaboration (isic). *arXiv preprint arXiv:1902.03368*, 2019.

[41] Allen Goodman, Anne Carpenter, Elizabeth Park, jlefman nvidia, Josette_BoozAllen, Kyle, Maggie, Nilofer, Peter Sedivec, and Will Cukierski. 2018 data science bowl. <https://kaggle.com/competitions/data-science-bowl-2018>, 2018. Kaggle.

[42] NVIDIA. Nvidia h100 tensor core gpu architecture. Whitepaper, 2022.

[43] Fengfu Li, Bin Liu, Xiaoxing Wang, Bo Zhang, and Junchi Yan. Ternary weight networks. *arXiv preprint arXiv:1605.04711*, 2016.

[44] Chenzhuo Zhu, Song Han, Huizi Mao, and William J Dally. Trained ternary quantization. *arXiv preprint arXiv:1612.01064*, 2016.

[45] Peng Chen, Bohan Zhuang, and Chunhua Shen. Fatnn: Fast and accurate ternary neural networks. In *Proceedings of the IEEE/CVF International Conference on Computer Vision*, pages 5219–5228, 2021.

[46] Huimin Huang, Lanfen Lin, Ruofeng Tong, Hongjie Hu, Qiaowei Zhang, Yutaro Iwamoto, Xianhua Han, Yen-Wei Chen, and Jian Wu. Unet 3+: A full-scale connected unet for medical image segmentation. In *ICASSP 2020-2020 IEEE international conference on acoustics, speech and signal processing (ICASSP)*, pages 1055–1059. Ieee, 2020.

[47] Ozan Oktay, Jo Schlemper, Loic Le Folgoc, Matthew Lee, Matthias Heinrich, Kazunari Misawa, Kensaku Mori, Steven McDonagh, Nils Y Hammerla, Bernhard Kainz, et al. Attention u-net: Learning where to look for the pancreas. *arXiv preprint arXiv:1804.03999*, 2018.

[48] Foivos I Diakogiannis, François Waldner, Peter Caccetta, and Chen Wu. Resunet-a: A deep learning framework for semantic segmentation of remotely sensed data. *ISPRS Journal of Photogrammetry and Remote Sensing*, 162:94–114, 2020.

[49] Md Zahangir Alom, Chris Yakopcic, Mahmudul Hasan, Tarek M Taha, and Vijayan K Asari. Recurrent residual u-net for medical image segmentation. *Journal of medical imaging*, 6(1):014006–014006, 2019.

[50] Robin Strudel, Ricardo Garcia, Ivan Laptev, and Cordelia Schmid. Segmenter: Transformer for semantic segmentation. In *Proceedings of the IEEE/CVF international conference on computer vision*, pages 7262–7272, 2021.

- [51] Alexander Kirillov, Eric Mintun, Nikhila Ravi, Hanzi Mao, Chloe Rolland, Laura Gustafson, Tete Xiao, Spencer Whitehead, Alexander C Berg, Wan-Yen Lo, et al. Segment anything. In *Proceedings of the IEEE/CVF international conference on computer vision*, pages 4015–4026, 2023.
- [52] Nikhila Ravi, Valentin Gabeur, Yuan-Ting Hu, Ronghang Hu, Chaitanya Ryali, Tengyu Ma, Haitham Khedr, Roman Rädle, Chloe Rolland, Laura Gustafson, et al. Sam 2: Segment anything in images and videos. *arXiv preprint arXiv:2408.00714*, 2024.
- [53] Chi-Mao Fan, Tsung-Jung Liu, and Kuan-Hsien Liu. Sunet: Swin transformer unet for image denoising. In *2022 IEEE International Symposium on Circuits and Systems (ISCAS)*, pages 2333–2337. IEEE, 2022.
- [54] Milan Tripathi. Facial image denoising using autoencoder and unet. *Heritage and Sustainable Development*, 3(2):89, 2021.
- [55] Xiaodan Hu, Mohamed A Naiel, Alexander Wong, Mark Lamm, and Paul Fieguth. Runet: A robust unet architecture for image super-resolution. In *Proceedings of the IEEE/CVF Conference on Computer Vision and Pattern Recognition Workshops*, pages 0–0, 2019.
- [56] Alexandre Chapiro, Dongyeon Kim, Yuta Asano, and Rafał K. Mantiuk. Ar-david: Augmented reality display artifact video dataset. *ACM Trans. Graph.*, 43(6), November 2024.
- [57] Robin Rombach, Andreas Blattmann, Dominik Lorenz, Patrick Esser, and Björn Ommer. High-resolution image synthesis with latent diffusion models. In *Proceedings of the IEEE/CVF conference on computer vision and pattern recognition*, pages 10684–10695, 2022.

A Appendix

A.1 Detailed MBU-Net Architecture

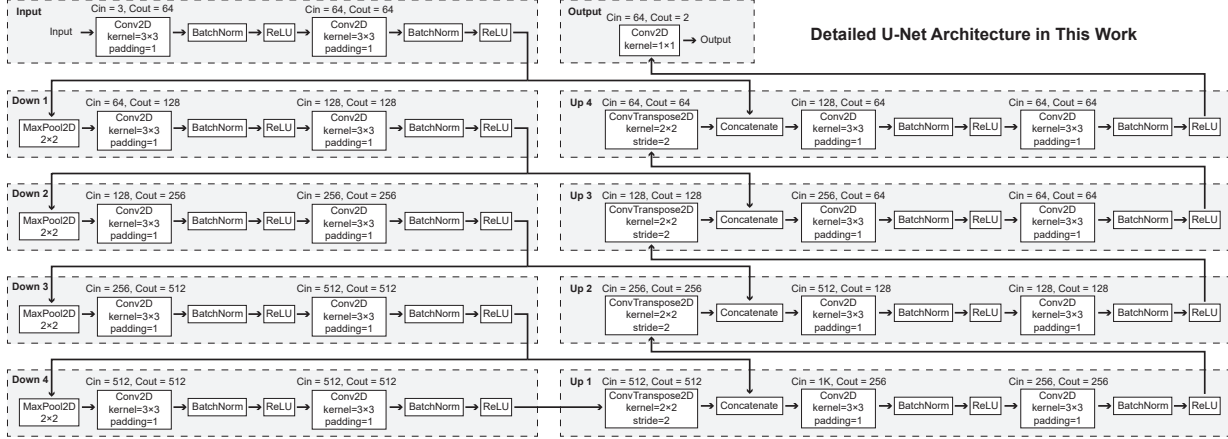


Figure A.1: The foundational U-Net architecture used in this work.

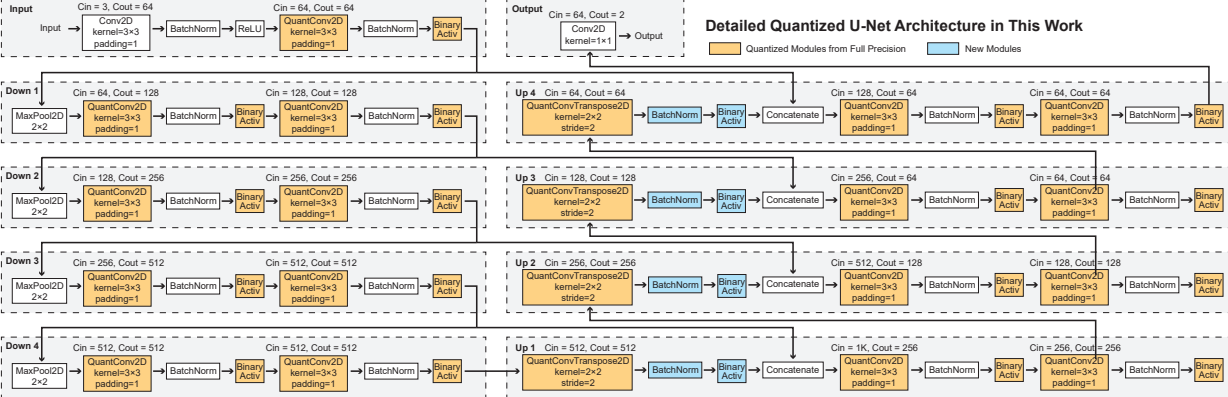


Figure A.2: The quantized U-Net architecture used in this work.

Figure A.1 and Figure A.2 illustrate the model architectures used in this work, with the former used to evaluate the full-precision configuration, and the other for quantized experiments. Compared to the foundational U-Net architecture, the quantized architecture not only modifies the ReLU activation function and the convolution/transposed convolution into binary versions, but also adds batchnorm and binary activation after transposed convolution layers to preserve the binary activation and ensure training quality.

A.2 Quantization Space Exploration

Figure A.3 shows the statistics of using higher bit quantization for individual convolution layers using Carvana dataset. The two input convolution layers, and the final convolution layer are full-precision (slightly different from the experiments in the main text, where the 2nd convolution layer is always masked-binary). In the first row, the four down-sampling layers are traversed from all binary to all 8-bit, totaling $4^4 = 256$ experiments, while the remaining layers are binary. Similarly, the second row traverses all double convolution layers in up-sampling with another 256 experiments. The distribution demonstrates that for most of the layers, the transition from binary to masked-binary contributes the most to accuracy, whereas negligible benefit is obtained from 2-bit to 4-bit, or from 4-bit to 8-bit. We thus confine the paper's scope within binary and 2-bit.

A.3 Training and Inference Configurations

A.3.1 Hyperparameters

Training and inference parameters are shown in Tables A.1 and A.2 list the hyperparameters. Full-precision training uses the RMSprop optimizer, while quantized training uses Adam.

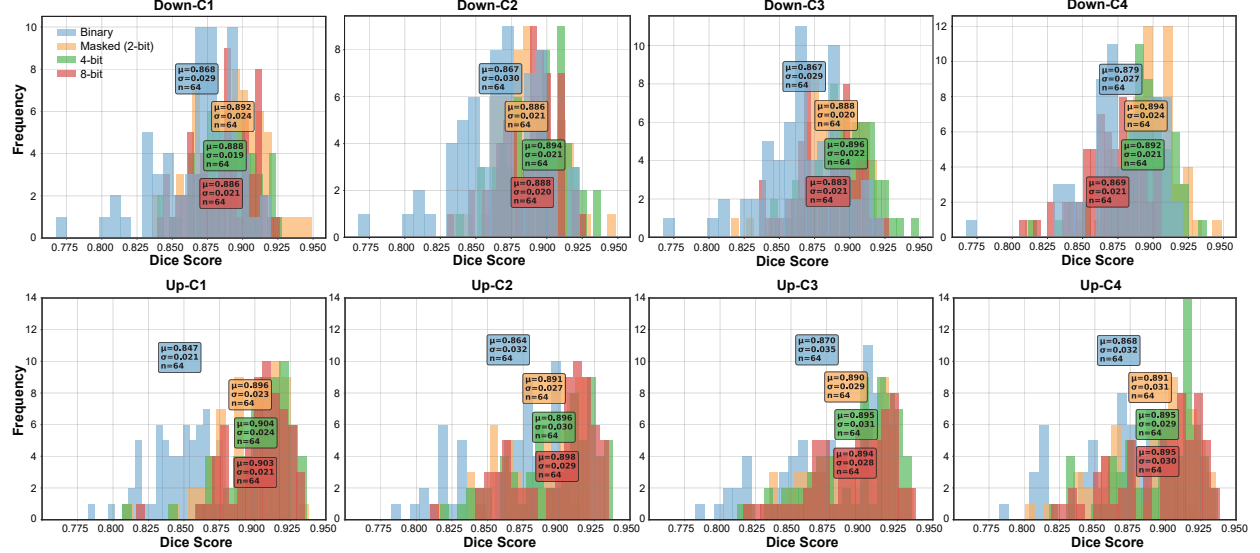


Figure A.3: Per-layer quantization space exploration. First row: Dice score distribution of 256 experiments on down-sampling convolution layers with binary remaining layers. Second row: distribution of 256 experiments on up-sampling convolution layers with binary remaining layers. Each sub-figure explores the accuracy improvement of increasing the number of bits for this layer’s weights.

Table A.1: The training hyperparameters for separate experiments.

Batch Size	Learning Rate	Number of Epochs	Grad Clipping	Weight Decay	Momentum
2	1e-5	30	1.0	1e-8	0.9

A.3.2 Dataset Details

Table A.3 shows the dimensions of the three selected datasets. The data are scaled from the original datasets to the numbers listed in the table. For Nuclei dataset, the original individual nucleus masks are combined into a comprehensive mask to facilitate the image-mask pair for segmentation.

A.4 Detailed Ablation Studies

A.4.1 Cost Ranking

The cost scores and rankings for individual layers of the U-Net used in this work are listed in Table A.4. In our ablation studies, the layers are gradually masked starting from Rank 1 to evaluate the tradeoff between efficiency and accuracy.

A.4.2 Results of Additional Metrics

Figure A.4 shows the Pareto frontiers of speed in FPS and accuracy in IoU and F1 score, on A100 GPU platform. The results are consistent with Figure 7 in the main text. Figure A.5 demonstrates the Pareto frontiers on other GPU platforms (H100, RTX 2080 Ti, and Jetson Orin Nano). On RTX 2080 Ti and Jetson Orin Nano, MBU-Net variations clearly outperforms FP32 and FP16 in terms of speed, while the accuracy drop is low when sufficient masked layers are deployed. As discussed in the main text, on H100, the performance of MBU-Net is lost due to the lack of BMMA support.

Table A.2: The batch sizes used for inference experiments. For fair comparison, the batch sizes for FP32 and FP16 are maximized before the GPUs run out of memory.

Dataset	Carvana			ISIC			Nuclei		
	FP32	FP16	MBU-Net	FP32	FP16	MBU-Net	FP32	FP16	MBU-Net
A100	32	32	64	64	128	128	64	128	128
H100	64	64	64	128	256	256	128	256	256
Jetson	4	8	32	8	16	64	8	16	64
2080 Ti	8	16	64	16	32	128	16	32	128

Table A.3: Dataset specifications.

Dataset	Number of Images	Width	Height
Carvana	5088	959	640
ISIC	3693	640	480
Nuclei	669	512	512

Table A.4: Cost scores and rankings of layers.

Rank	Layer	Cost Score	Rank	Layer	Cost Score	Rank	Layer	Cost Score
1	Up-CT4	0.011	5	Up-C3	0.228	9	Up-C4	0.512
2	Up-CT3	0.016	6	Down-C1	0.273	10	Up-C1	0.521
3	Up-CT2	0.037	7	Up-C2	0.286	11	Down-C4	0.583
4	Up-CT1	0.120	8	Down-C2	0.406	12	Down-C3	0.625

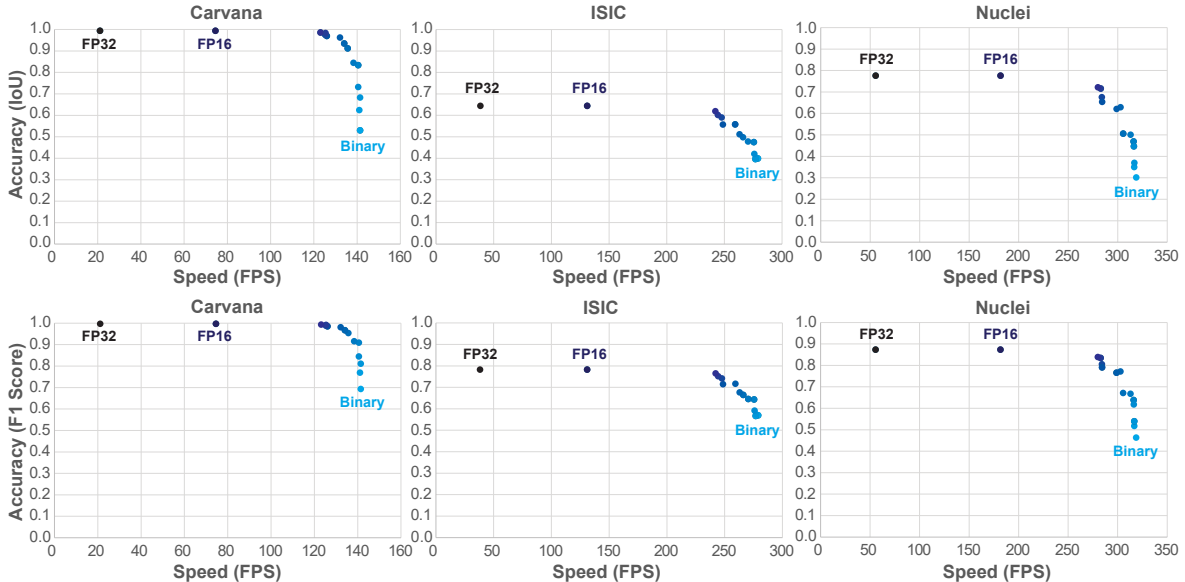


Figure A.4: Speed vs. accuracy (IoU and F1 score) on A100.

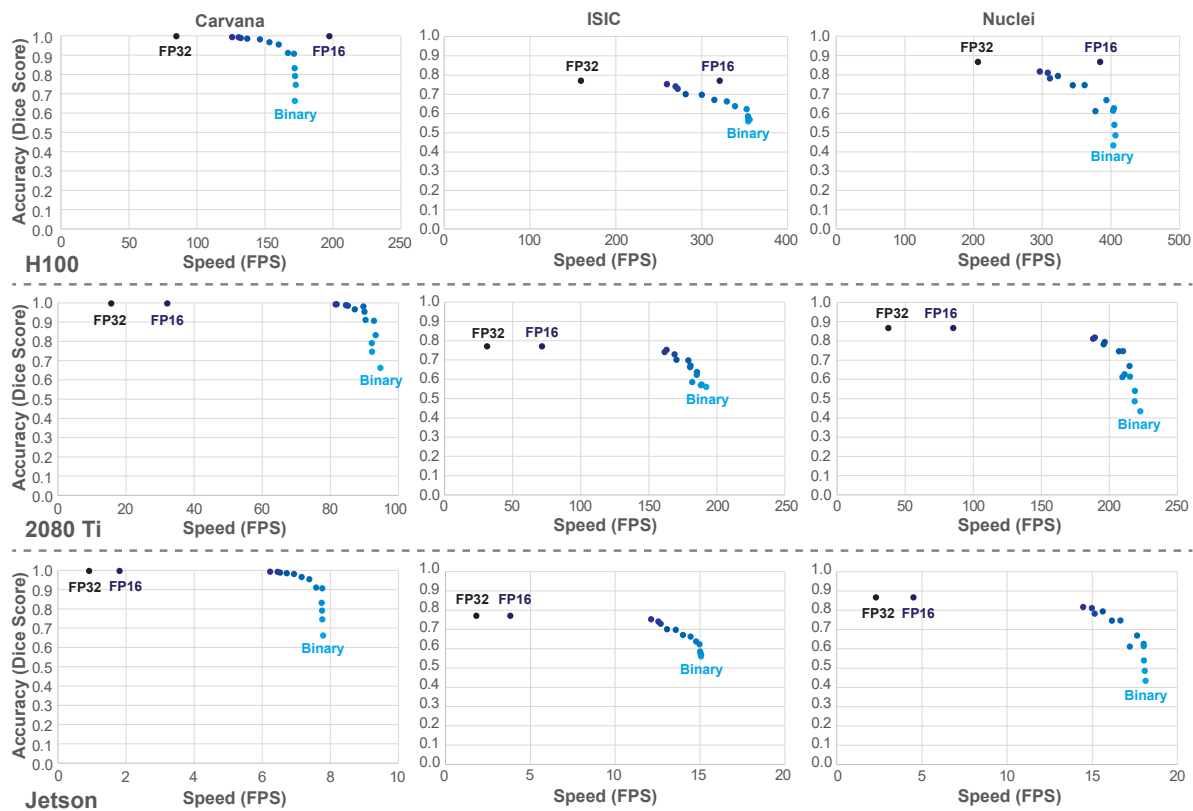


Figure A.5: Speed vs. accuracy (Dice score) on H100, RTX 2080 Ti, and Jetson Orin Nano.